ChemComm

Accepted Manuscript

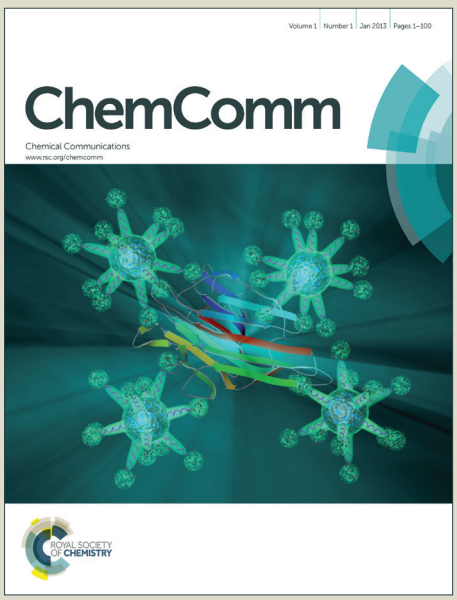

ROYAL SOCIETY OF CHEMISTRY

www.rsc.org/chemcomm

ChemComm

RSCPublishing

COMMUNICATION

Thickness-dependent SERS activities of gold nanosheets controllably synthesized *via* photochemical reduction in lamellar liquid crystals

Cite this: DOI: 10.1039/x0xx00000x

Received 00th January 2014,
Accepted 00th January 2014

DOI: 10.1039/x0xx00000x

www.rsc.org/

Man Zhou,[a] Ming Lin,[b] Lie Chen,[a] Yongzheng Wang,[a] Xiangke Guo,[a] Luming Peng,[a] Xuefeng Guo,*[a] and Weiping Ding[a]

Gold nanosheets (AuNSs) with well-tuned thicknesses were synthesized by a facile photochemical reduction method in lamellar liquid crystals. It is found that ~50 nm thick AuNSs present much stronger surface-enhanced Raman scattering (SERS) effect than that of AuNSs with thickness of ~8 nm and 100 nm.

Since the discovery of surface-enhanced Raman scattering (SERS) effect in the 1970s,[1-3] SERS spectroscopy has arisen as one of the most powerful tools for ultrasensitive detection.[4-6] Numerous studies have demonstrated that nanostructured Ag, Au and Cu are important candidates for SERS applications. To improve SERS signals, various nanostructures including cubes,[7] stars,[8] rods,[9] wires[10] and plates[11] have emerged as SERS-active substrates. Recently, complicated substrates have been fabricated for the amplification of SERS signals.[12-14] The related investigations have revealed that the performances of SERS-active substrates critically depend on the size and morphology[15,16] Hence, simply fabricating uniform and high sensitive SERS substrates is highly desired for their wide applications.

In the past decade, two-dimensional (2D) nanomaterials have attracted increasing attentions because of their unique physical and chemical properties.[17,18] Among all these 2D nanomaterials, gold nanosheets (AuNSs) are of particular interest owing to their remarkable properties, such as high conductivity, ultrasmooth surface and unique surface plasmon polaritons (SPPs) feature. As a result, the application of AuNSs covers many fields, including plasmonics, electronics, biosensors, *etc*.[19-21] Various strategies have been developed for the fabrication of AuNSs (*i.e.*, wet chemical, photochemical, electrochemical and sonochemical routes). Since Au is nonlayered material, however, it's hard to achieve thickness-controlled synthesis of Au nanosheets due to the lack of controllable means of inducing anisotropic growth of 2D structures. Very recently, Qin et al. reported a thickness-controlled synthesis of ultrathin Au nanosheets with thickness from 5 to 40 nm, in which a home-made nonionic surfactant dodecylglyceryl itaconate (DGI) were used as template.[22] So far, although AuNSs with various morphologies have been synthesized via different synthetic processes, the controllable and simple fabrication of AuNSs with different thicknesses in a large size range and their SERS activities are still far less investigated.

Herein, we report a facile one-step route to controllably synthesize AuNSs through photochemical reactions with lyotropic liquid crystals (LCs) as a soft template. The LCs system contained lamellar bilayer membranes formed by Tween 40 (polyoxyethylene sorbitan monopalmitate), CSA (camphorsulfonic acid) and water. As reported by us before,[23,24] the lamellar LCs was used as template for the synthesis of noncrystalline metal-boron nanotubes through a rolling-up procedure. Here the lamellar LCs system is extended for the photochemical synthesis of AuNSs with well-tuned thicknesses. We also find that sunlight is an optimum and green light source for the production of AuNSs from the reduction of chloroauric acid. Furthermore, three kinds of AuNSs with different thicknesses were tested to compare their SERS abilities with Rhodamine 6G (R6G) as a probe molecule. A remarkable thickness-dependent SERS effect of gold nanosheets was discovered.

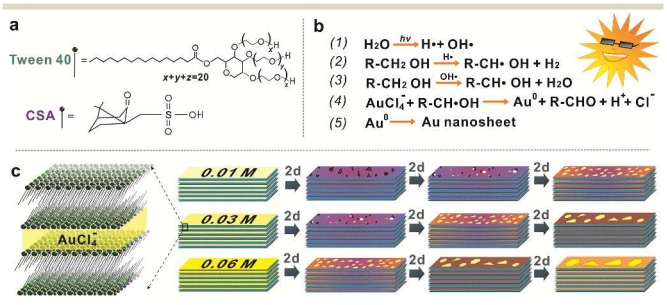

Fig. 1 (a) Structural formulas of Tween 40 and CSA; (b) Main steps of photochemical reaction; (c) Schematic diagram of the formation of AuNSs within LCs templates using 0.01 M, 0.03 M and 0.06 M $HAuCl_4$.

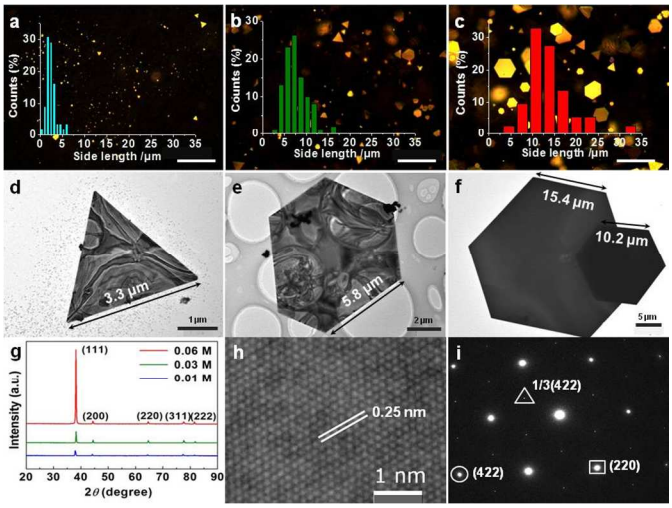

Fig. 2 (a-c) Size distribution histograms of AuNSs calculated from corresponding optical images (scale bars: 50 μm), (a) 0.01 M, (b) 0.03 M, (c) 0.06 M $HAuCl_4$. (d-f) Representative TEM images of the AuNSs obtained with (d) 0.01 M, (e) 0.03 M, (f) 0.06 M $HAuCl_4$. (g) XRD patterns of the AuNSs obtained with different HAuCl4 concentrations; (h) HRTEM image and (i) corresponding SAED pattern of the AuNSs obtained with 0.06 M $HAuCl_4$.

The schematic diagram for the photochemical synthesis of AuNSs with well-tuned thicknesses is shown in Fig. 1. As illustrated in Fig. 1b and 1c, after being excited by the sunlight, H·/OH· radicals generated within water layers and then attacked the $-CH_2OH$ groups of Tween 40 molecules to produce an appropriate amount of -CH·OH radicals, which had strong reducing property.[25] Finally, $AuCl_4^{-1}$ ions were reduced to Au^0 nanoseeds and gradually grew into small single-crystalline AuNSs under the limitation and stabilization by the lamellar LCs. The LCs acted as the morphology directing agent for the Au nanosheets during the whole photochemical reduction process. Both irradiation time and concentration of chloroauric acid ($HAuCl_4$) are the controlling factors for inducing anisotropic growth of AuNSs (see Fig. 1c and Fig. S1, ESI†). For a simple presentation, size and thickness adjustment was carried out only by varying the concentration of $HAuCl_4$ in this work. It indicated that the precursor chloroauric acid ($HAuCl_4$) was stable without the irradiation of sunlight. By contrast, the direct sunlight and UV light with high irradiation power density resulted in large amounts of unwanted Au nanoparticles which were difficult to be separated from the obtained AuNSs (see Fig. S2 and Table S1, ESI†). This might be attributed to the fast reduction rate caused by the pure and strong UV light. The strength of light irradiation was one of the key factors for the highly efficient growth of AuNSs, and the natural sunlight was found as an optimum and green light source for the production of AuNSs in the present synthesis.

Three kinds of AuNSs with different sizes were obtained under the same condition of 6 days' irradiation except the different concentrations of $HAuCl_4$ (0.01 M, 0.03 M and 0.06 M). Before the obtained AuNSs were washed alternately with ethanol and hot water to remove Tween 40 and CSA, optical microscope images were taken in situ to demonstrate the relationship between side lengths and precursor concentrations. When using 0.01 M $HAuCl_4$, the average side length of nanosheets was about 2.5 μm with a narrow size distribution (see Fig. 2a). While the concentration of $HAuCl_4$ increased from 0.03 M to 0.06 M, the average size grew from 7.5 μm to 13.5 μm and the size distribution became wider (see Fig. 2b-2c). More optical microscope images can be seen in Fig. S3, ESI†. Furthermore, an approximate linear relationship between sizes and concentrations was found and shown in Fig. S4, ESI†. It indicates that sizes of AuNSs could be effectively controlled by adjusting $HAuCl_4$ concentrations. Fig. 2d-2f show the representative transmission electron microscopy (TEM) images of AuNSs with side lengths of 3.3 μm, 5.8 μm, 10.2 μm and 15.4 μm. Fig. 2g shows the X-ray diffraction (XRD) patterns of the AuNSs obtained with different $HAuCl_4$ concentrations. Diffraction peaks of (111), (200), (220), (311) and (222) can be clearly seen to prove the face-centred cubic (fcc) crystal of gold, among which the {111} facets are the dominating facets, as indicated by the amazing strong (111) diffraction peak and its secondary (222) diffraction peak. The extremely low (200)/(111) relative diffraction intensity value of the obtained AuNSs with 0.06 M $HAuCl_4$ is 0.035, which is much lower than the Au bulk value (0.52, JCPDS 04-0784), suggesting a preferred orientation of Au nanosheets in the (111) direction. Moreover, a contrastive analysis of AuNSs using different $HAuCl_4$ concentrations shows that the relative diffraction intensities of (200)/(111) and (220)/(111) decrease with increased size of AuNSs, indicating that the preferred orientation of the (111) direction in larger size AuNSs is further intensified. A typical high-resolution TEM (HRTEM) image of the obtained AuNSs with 0.06 M $HAuCl_4$ reveals it is single crystalline with a fringe spacing of 0.25 nm, which corresponds to 1/3{422} reflection (see Fig. 2h).[26] As shown in Fig. 2i, the hexagonal diffraction spots further confirm that AuNSs are single crystal with highly oriented (111) planes. In addition, the inner spots (triangled in Fig. 2i) with a weaker intensity correspond to the formally forbidden 1/3{422} reflection, which indicates that the surface of the AuNSs is atomically flat.[27,28]

The thickness of nanosheets is simultaneously changed with the lateral size together by adjusting the concentration of $HAuCl_4$. Fig. 3 shows three typical atomic force microscopy (AFM) images of AuNSs with approximate thicknesses of 8 nm, 50 nm, and 100 nm. More detailed analysis of the thickness distributions was done using an optical imaging method combined with image analysis software (see Fig. S5, ESI†). It is clear that the thicknesses of the obtained AuNSs increased with increasing the concentrations of $HAuCl_4$ (see Fig. S6, ESI†). Due to the curling up phenomena of the ultrathin unstable edges, the section analysis curves of the AuNSs showed that the edges seem thicker than in the middle (see Fig. S7, ESI†). To simplify the description later, these three samples with approximate thicknesses of 8 nm, 50 nm and 100 nm were denoted as AuNSs-8, AuNSs-50 and AuNSs-100, respectively.

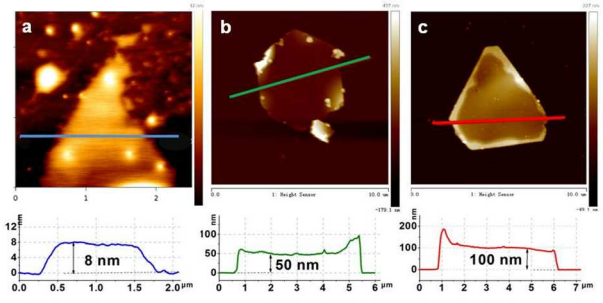

Fig. 3 Representative AFM images of AuNSs using different $HAuCl_4$ concentrations: (a) 0.01 M; (b) 0.03 M and (c) 0.06 M.

The uniform single-crystalline AuNSs with well-tuned thicknesses in a large size range inspired us to investigate their SERS activities. Rhodamine 6G (R6G) was chosen as a probe molecule and used with different concentrations (10^{-5} M, 10^{-6} M and 10^{-8} M). Fig. 4 shows a series of SERS spectra of R6G on the AuNSs. Raman peaks observed at 609, 770, 1181, 1309, 1358, 1507, 1572, and 1644 cm^{-1} were consistent with the reported Raman signals of R6G calculated by Schatz et al.[29] The assignments of vibrations are listed in Table S2 in the Supporting Information. The SERS intensities increased with the increasing R6G concentrations. The SERS intensity for the different AuNSs thicknesses were monitored at two different Raman peaks, *i.e.*, the Raman peaks of 1358 cm^{-1} (xanthenes ring stretching and in plane C-H bending) and 1507 cm^{-1} (xanthenes ring stretching) for R6G. In the case of 10^{-5} M R6G, as clearly shown in Fig. 4a, the SERS intensities of AuNSs-50 were 5 times and 23 times higher than that of AuNSs-8 and AuNSs-100, respectively. 10^{-6} M and 10^{-8} M of R6G were tested under the same condition to further confirm this order of enhancement ability, of which maximum enhancement occurs on the surface of AuNSs-50 (see Fig. 4b). Even when the concentration of R6G was further lowered to 10^{-8} M, peaks at 1358 and 1507 cm^{-1} were still visible using AuNSs-50 as SERS substrates. By contrast, the singles of R6G molecules on the surfaces of AuNSs-8 and AuNSs-100 were almost invisible (see Fig. 4c). So it was proved that R6G can be confidently detected as low as 10^{-8} M. The order of thickness-dependent SERS activities of the obtained AuNSs is AuNSs-50 > AuNSs-8 > AuNSs-100. We expect that a suitable thickness and size could maximize the electromagnetic enhancement effect (EM) which makes the main contribution to the SERS enhancement.[5]

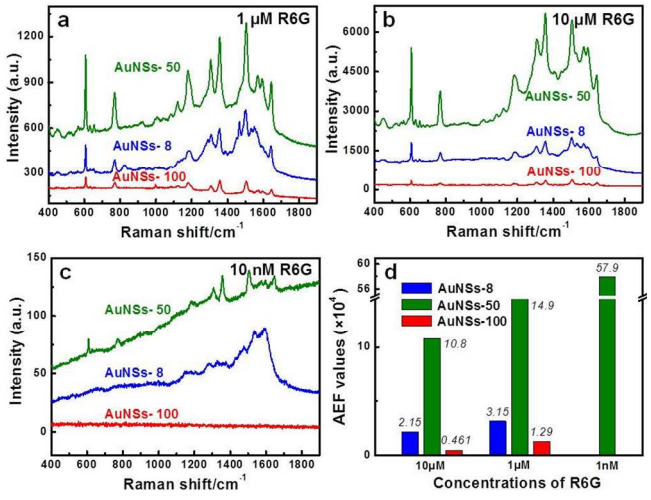

Fig. 4 Surface enhanced Raman scattering (SERS) using AuNSs-8, AuNSs-50 and AuNSs-100. SERS spectra recorded for (a) 10 μM; (b) 1 μM; (c) 10 nM R6G in ethanol; (d) AEF values of AuNSs-8, AuNSs-50 and AuNSs-100.

Using data of SERS experiments, the analytical enhancement factor (AEF) was calculated followed the method used by Chiu[30], which defined by the equation AEF = $(I_{SERS}/C_{SERS})/(I_{RS}/C_{RS})$. Here, I_{SERS} is the SERS intensity of R6G on the AuNSs; C_{SERS} is the concentration of R6G; while I_{RS} stands for the Raman intensity of R6G on a non-SERS active glass substrate (slide). Based on above experimental data, the AEF values are calculated by calculating the SERS intensities at 1358 cm^{-1} and 1507 cm^{-1}. The AEF values of AuNSs-50, AuNSs-8, and AuNSs-100 are 1.1×10^5, 2.2×10^4 and 4.6×10^3, respectively (see Fig. 4d). The details of calculations can be seen in Table S3-S4.

In summary, a facile one-pot photochemical method has been successfully developed to prepare a series of crystalline AuNSs with controllable thicknesses. This photochemical reduction can be convenient performed under ambient conditions at room temperature which involved no extra reducing agent but only natural sunlight. Three kinds of typical AuNSs (AuNSs-8, AuNS-50 and AuNSs-100) with micrometer-scale size and well-tuned thickness were obtained by adjusting the concentration of $HAuCl_4$. Furthermore, the SERS effects of these AuNSs were investigated, and a remarkable thickness-dependent SERS effect of gold nanosheets with order of AuNSs-50 > AuNSs-8 > AuNSs-100 was discovered. The present facile controllable synthesis of Au nanosheets and the thickness-dependent SERS activities may open up a range of possible applications in the design of 2D materials-based high performance SERS substrates.

Acknowledgment

This work was financially supported by the National Basic Research Program (2009CB623504), the National Science Foundation of China (21173119, 21273109, 21303083), the Natural Science Foundation of Jiangsu Province (BK20130563), the Specialized Research Fund for the Doctoral Program of Higher Education (20130091120045) and the Fundamental Research Funds for the Central Universities.

Notes and references

[*a] *Key Laboratory of Mesoscopic Chemistry of MOE, School of Chemistry and Chemical Engineering, Nanjing University, Nanjing 210093, China*
E-mail: guoxf@nju.edu.cn.

[b] *Institute of Materials Research & Engineering, A*STAR (Agency for Science, Technology and Research), 3 Research Link, Singapore 117602, Singapore.*

† Electronic Supplementary Information (ESI) available: more details of synthesis and characterizations including TEM, SEM, AFM images as well as AEF calculations. See DOI: 10.1039/b000000x/

1 M. Fleischmann, P. J. Hendra and A. J. McQuillan, *Chem. Phys. Lett.*, 1974, **26**, 163.
2 M. G. Albrecht, and J. A. Creighton, *J. Am. Chem. Soc.*, 1977, **99**, 5215.
3. D. L. Jeanmaire, , and R. P.Van Duyne, *J. Electroanal. Chem.*, 1977, **84**, 1.
4. K. Kneipp, Y. Wang, H. Kneipp, L. T. Perelman, I. Itzkan, R. Dasari and M. S. Feld, *Phys.Rev.Lett.*, 1997, **78**, 1667.
5. W. G. Xu, X. Ling, J. Q. Xiao, M. S. Dresselhaus, J. Kong, H. X. Xu, Z. F. Liu and J. Zhang, *Proc. Natl. Acad. Sci. U.S.A.*, 2012, **109**, 9281.
6. W. Ma, M. Z. Sun, L. G. Xu, L. B. Wang, H. Kuang and C. L. Xu, *Chem. Commun.*, 2013, **49**, 4989.
7. P.H.C. Camargo, M. Rycenga, L. Au and Y. N. Xia, *Angew. Chem., Int.Ed.*, 2009, **48**, 2080.
8. E. N. Esenturk and A. R. H. Walker, *J. Raman Spectrosc*, 2009, **40**, 86.
9. C. J. Murphy, A. M. Gole, S. E. Hunyadi, J. W. Stone, P. N. Sisco, A. Alkilany, B. E. Kinard and P. Hankins, *Chem. Commun.*, 2008, **5**, 544.
10. I. Yoon, T. Kang, W. Choi, J. Kim, Y. Yoo, S. W. Joo, Q. H. Park, H. Ihee and B. Kim, *J. Am. Chem. Soc.*, 2009, **131**, 758.
11. Y. G. Sun and G. P. Wiederrecht, *Small*, 2007, **3**, 1964.

12. J. Li, Y. Huang, Y. Ding, Z. Yang, S. Li, X. Zhou, F. Fan, W. Zhang, Z. Zhou, D. Wu, B. Ren, Z. Wang and Z. Tian, *Nature,* 2010, **464**, 392.
13. J. M. McLellan, Z. Li, A. R. Siekkinen and Y. N. Xia, *Nano Lett.*, 2007, **7**, 1013.
14. K. Ikeda, S. Suzuki and K. Uosaki, *J. Am. Chem. Soc.*, 2013, **135**, 17387.
15 N. R. Jana and T. Pal, *Adv. Mater.*, 2007, **19**, 1761.
16 R. N. Cassar, D. Graham, I. Larmour, A. W. Wark and K. Faulds, *Vib. Spectrosc.*, 2014, **71**, 41.
17. P. Miró, M. Audiffred and T. Heine, *Chem. Soc. Rev.*, 2014, **43**, 6537.
18. M. S. Xu, T. Liang, M. M. Shi and H. Z. Chen, *Chem. Rev.*, 2013, **113**, 3766.
19. T. A. Major, M. S. Devadas, S. S. Lo and G. V. Hartland. *J. Phys. Chem. C.*, 2013, **117**, 1447.
20. G. D. Moon, G. H. Lim, J. H. Song, M. Shin, T. Yu, B. Lim and U. Jeong, *Adv. Mater.*, 2013, **25**, 2707.
21. S. R. Beeram and F. P. Zamborini, *J. Am. Chem. Soc.*, 2009, **131**, 11689.
22. H. L. Qin, D. Wang, Z. L. Huang, D. M. Wu, Z. C. Zeng, B. Ren, K. Xu and J. Jin, *J. Am. Chem. Soc.*, 2013, **135**, 12544.
23. Y. Zhu, F. P. Liu, W. P. Ding, X. F. Guo and Y. Chen, *Angew. Chem., Int.Ed.*, 2006, **118**, 7369.
24. M. Mo, L. Han, J. G. Lv, Y. Zhu, L. M. Peng, X. F. Guo and W. P. Ding, *Chem. Commun.*, 2010, **46**, 2268.
25. K. Mallik; M. Mandal; N. Pradhan and T. Pal, *Nano Lett.* 2001, **1**, 319.
26. X. Bai, L. Zheng, N. Li, B. Dong and H. Liu. *Cryst. Growth Des.* 2010, **8**, 3840.
27. J. P. Xie, J. Y. Lee, D. I. C. Wang and Y. P. Ting, *Small*, 2007, **3**, 672.
28. S. Nootchanat, C. Thammacharoen, B. Lohwongwatana, and S. Ekgasit, *RSC Adv.*, 2013, **3**, 3707.
29. L. Jensen and G. C. Schatz, *J. Phys. Chem. A.*, 2006, **110**, 5973.

